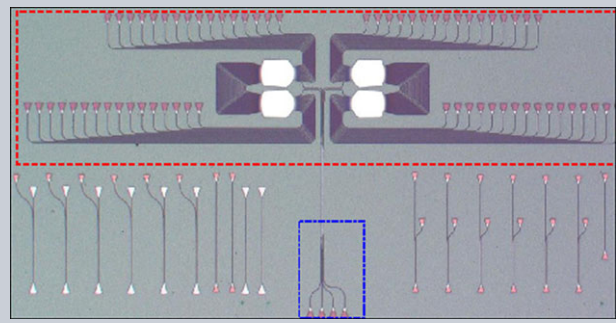


**Abstract** A compact 64-channel hybrid demultiplexer based on silicon-on-insulator nanowires is proposed and demonstrated experimentally to enable wavelength-division-multiplexing and mode-division-multiplexing simultaneously in order to realize an ultra-large capacity on-chip optical-interconnect link. The present hybrid demultiplexer consists of a 4-channel mode multiplexer constructed with cascaded asymmetrical directional-couplers and two bi-directional  $17 \times 17$  arrayed-waveguide gratings (AWGs) with 16 channels. Here each bi-directional AWG is equivalent as two identical  $1 \times 16$  AWGs. The measured excess loss and the crosstalk for the monolithically integrated 64-channel hybrid demultiplexer are about -5 dB and -14 dB, respectively. Better performance can be achieved by minimizing the imperfections (particularly in AWGs) during the fabrication processes.



# Monolithically integrated 64-channel silicon hybrid demultiplexer enabling simultaneous wavelength- and mode-division-multiplexing

Daoxin Dai\*, Jian Wang, Sitao Chen, Shipeng Wang, and Sailing He

## 1. Introduction

The optical interconnect has been attracting intensive attention due to its potential to achieve a very high link capacity. Particularly, the link capacity over a single optical fiber or waveguide can be further improved by utilizing various advanced multiplexing technologies [1]. Among them, the wavelength-division-multiplexing (WDM) technique, utilizing many wavelength channels, is one of the most popular technologies and has been developed very successfully in the past decades, not only for long-distance optical fiber communication system but also for short-distance optical interconnects [2]. In a WDM system, many laser sources are needed, and thus the cost for the hardware as well as for the management might be too expensive to be affordable. Recently, mode-division-multiplexing (MDM) technology utilizing multiple orthogonal guided-modes in a multimode fiber or waveguide has received intensive attention for fiber optical communications as well as on-chip optical interconnects due to its benefits to the capacity of a single-wavelength carrier [3]–[4]. For an MDM system, the key component is the mode (de)multiplexer, which combines/separates the signals carried by different mode-channels. In recent years, various mode (de)multiplexers have been developed successfully by using multimode interference (MMI) couplers [5]–[6], adiabatic mode-evolution couplers [7], an asymmetrical Y-junction [8–10], and asymmetrical directional couplers (ADCs) [11–19]. The ADC-

based mode (de)multiplexer is an attractive option because of the broad wavelength band, the small footprint and the scalability. Previously, a 4-channel mode (de)multiplexer with excellent performance has been demonstrated by using cascaded ADCs [14].

It is even more interesting to improve the capacity of an optical-interconnect link further to even Peta-bits/s by utilizing a multi-dimensional hybrid multiplexing technology, which combines several multiplexing technologies together compatibly [1], and the key component is the hybrid (de)multiplexer. An 8-channel hybrid multiplexer has been proposed and demonstrated to enable the MDM and PDM (polarization-division-multiplexing) technologies simultaneously [17]–[18]. Recently there are also some impressive experiments demonstrating an MDM-WDM link with a few modes and wavelengths, as summarized in Table 1. For example, a 2-mode  $\times$  3-wavelength MDM-WDM link with a wavelength channel spacing  $\Delta\lambda_{\text{ch}}$  as large as 15 ~ 16 nm was demonstrated by using the (de)multiplexer based on ADC-assisted microrings in Ref. [19]. In [20], a mode multiplexer based on an asymmetrical Y-junction was used to realize a 2-mode  $\times$  3-wavelength MDM-WDM optical link with  $\Delta\lambda_{\text{ch}} = 8 \sim 10$  nm. More recently, a SiN mode (de)multiplexer based on ADC-assisted microrings was demonstrated for realizing MDM-WDM link [21]. These experimental results prove the capability of the mode (de)multiplexer to work in a WDM system. However, in these experiments

Centre for Optical and Electromagnetic Research, State Key Laboratory for Modern Optical Instrumentation, Zhejiang Provincial Key Laboratory for Sensing Technologies, Zhejiang University, Zijingang Campus, Hangzhou, 310058, China

\*Corresponding author: e-mail: dx dai@zju.edu.cn

**Table 1** Hybrid demultiplexing technologies enabling WDM and MDM.

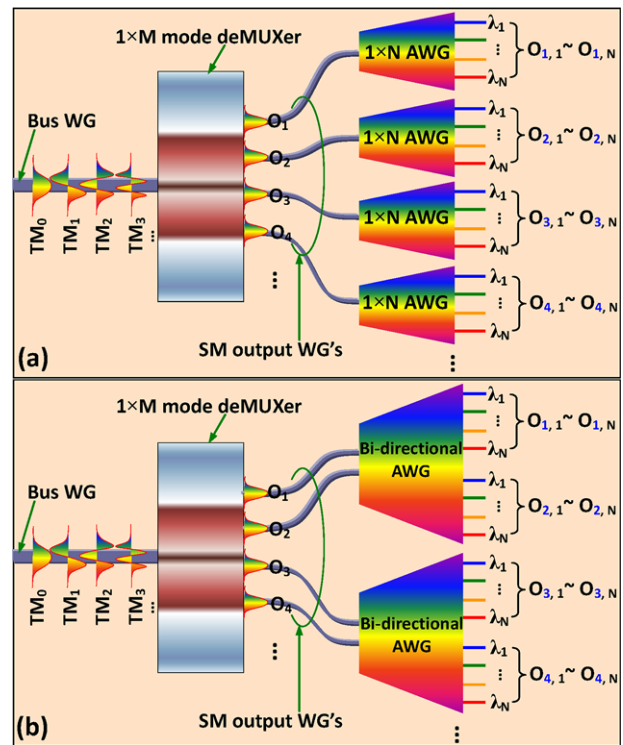
Reference #.	[19]	[20]	[21]	[22]	The present
Mode-channel number	2	2	3	4	4
Wavelength-channel number	3	3	1	16	16
$\Delta\lambda_{\text{ch}}$ (nm)	15, 16	8, 10	/	$\sim 3.2$	$\sim 3.2$
$\lambda$ -channel crosstalk (dB)	/	/	/	$\sim -10$	$\sim -14$
Mode-channel crosstalk (dB)	-22, -18, -12	$\sim -30$	-10, -15, -24	$\sim -20$	$\sim -20$
Excess loss (dB)	3 ~ 16	/	/	$\sim 7$	3.5 ~ 5.5

the total channel number is very limited and the channel spacing is pretty large ( $\sim 10$  nm; see Table 1). Furthermore, there are few demonstrations for the realization of monolithically integrated hybrid demultiplexer enabling simultaneous multi-channel MDM and WDM.

Recently, we proposed and demonstrated a monolithically integrated 64-channel hybrid demultiplexer on silicon by combining a  $1 \times 4$  mode demultiplexer and *four* identical arrayed-waveguide gratings (AWGs) for the first time [22]. Each AWG has 16 channels, and the wavelength-channel spacing is as small as 3.2 nm. Note that an  $N \times N$  AWG can work bi-directionally. Previously a silica  $N \times N$  bi-directional AWG with loop-back optical paths had been utilized to achieve an add-drop multiplexer [23]. For a bi-directional AWG, the insertion loss increases a little because the input waveguide is positioned at the edge [24]. Fortunately, the performance degradation is acceptable and excellent bi-directional AWGs have been demonstrated [25]. In this paper, we propose a novel silicon hybrid demultiplexer with  $(N + 1) \times (N + 1)$  bi-directional AWGs that can play the role of two identical  $1 \times N$  AWGs equivalently. In this way, the number of the AWGs needed for the hybrid demultiplexer is reduced by half. As an example, a 64-channel MDM-WDM hybrid demultiplexer is realized by integrating a  $1 \times 4$  ADC-type mode demultiplexer (with 4 mode-channels) and two  $17 \times 17$  bi-directional AWGs (with 16 wavelength-channels). With the proposed design, a very compact hybrid demultiplexer with excellent performance is realized, and the issue of the channel-wavelength's misalignment is also greatly reduced since only two AWGs are involved in comparison with the previous design with *four* AWGs demonstrated in [22].

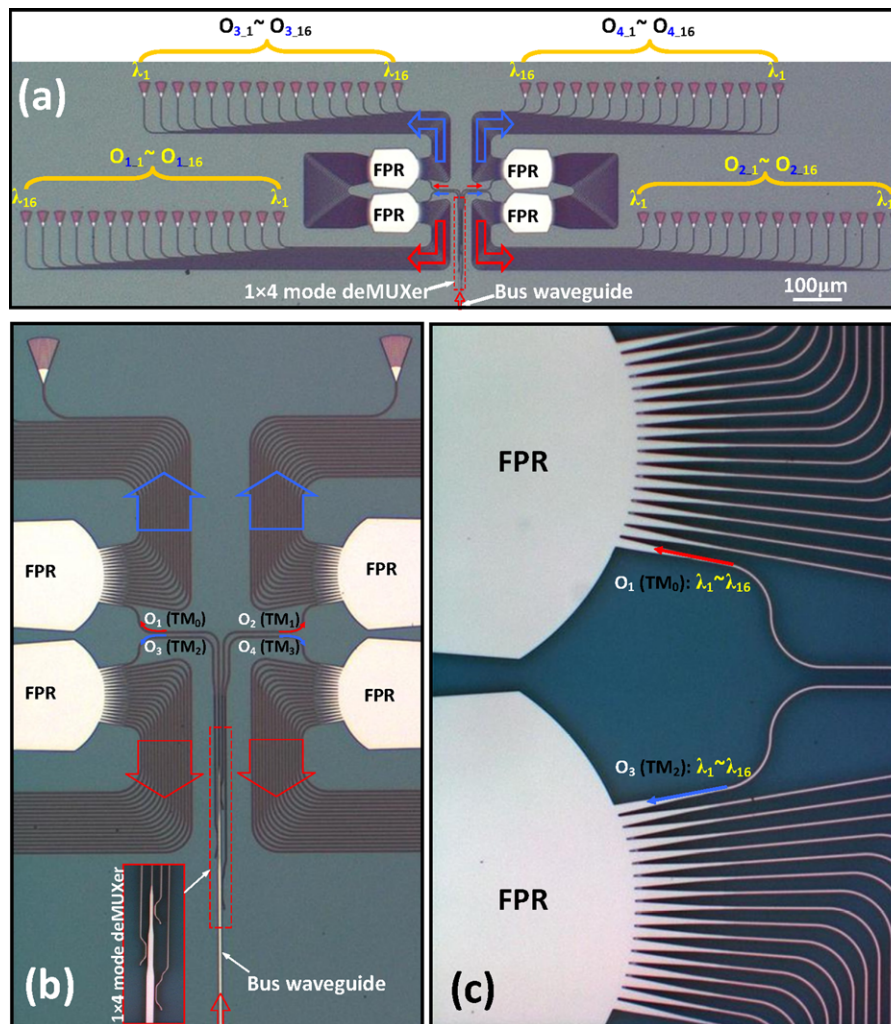
## 2. Structure, fabrication and characterization

Figure 1(a) shows the previous configuration for the two-dimensional hybrid demultiplexer, including a mode demultiplexer with  $M$  mode-channels and  $M$  wavelength-division-demultiplexers with  $N$  wavelength-channels (e.g.  $1 \times N$  AWGs [22]). The novel hybrid demultiplexer proposed in this paper is shown in Fig. 1(b), in which there are a  $1 \times M$  mode demultiplexer and  $M/2$  bi-directional  $(N + 1) \times (N + 1)$  AWGs. The  $1 \times M$  mode demultiplexer has a bus waveguide (which is multimode in order to sup-



**Figure 1** (a) A hybrid demultiplexer enabling MDM and WDM simultaneously with a  $1 \times M$  mode demultiplexer and  $M$  wavelength-division-demultiplexers with  $N$  channels (like  $1 \times N$  AWGs) [22]. (b) The present hybrid demultiplexer with a  $1 \times M$  mode demultiplexer and  $M/2$  bidirectional AWGs.  $M$  is the mode-channel number, and  $N$  is the wavelength-channel number.

port the propagation of the  $M$  mode-channels) and  $M$  single-mode output waveguides. The launched  $M$  mode-channels in the bus waveguide are separated and coupled to the fundamental mode of the  $M$  singlemode output waveguides, so that the regular bi-directional AWGs operating with the fundamental mode can be utilized. Note that any single-mode output waveguide of the  $1 \times M$  mode demultiplexer carries  $N$  wavelength-channels, which are demultiplexed by the cascaded bi-directional AWGs and output from the corresponding ports ( $O_{1,1} \sim O_{1,N}$ ,  $O_{2,1} \sim O_{2,N}$ , ...). In this way, the total channel number of the proposed hybrid demultiplexer is  $M \times N$  while the number of AWGs needed is  $M/2$  only ( $M$  is the mode-channel number) since each



**Figure 2** Optical microscopy pictures for the proposed hybrid demultiplexer including a 4-channel mode demultiplexer and two identical bi-directional AWGs with 16 channels. (a) The whole structure, (b) the enlarged view for the part including the  $1 \times 4$  mode demultiplexer, and (c) the enlarged view for the part including the FPRs and the input waveguides.

bi-directional  $(N + 1) \times (N + 1)$  AWG has two input waveguides and can deal with the signals from any two mode-channels.

As an example, we consider the case with four mode-channels and 16 wavelength-channels, i.e.,  $M = 4$  and  $N = 16$ , so that there are 64 channels available. For this case, only two  $17 \times 17$  bidirectional AWGs are needed, as shown in Fig. 2(a). All 64 channels carried by the four modes (the  $TM_0$ ,  $TM_1$ ,  $TM_2$ , and  $TM_3$  modes) and 16 wavelengths ( $\lambda_1, \dots, \lambda_{16}$ ) are first mode-demultiplexed into four groups, each of which has 16 wavelength-channels. These signals carried by the  $i$ -th mode-channel are further demultiplexed by the corresponding bi-directional AWG and output from ports  $O_{i-1} \sim O_{i-16}$ . As shown in Fig. 2(a)–(c), the bi-directional AWG has 28 arrayed waveguides, the ends of each of which are connected with two identical free propagation regions (FPRs). For any one of the FPRs, there are 17 access optical waveguides arranged uniformly along the Rowland circle, as shown in Fig. 2(a). Among these 17 access optical waveguides, the waveguide at the edge is chosen as the input waveguide for the AWG while the other 16 access waveguides are used as the output waveguides for

light launched from the input waveguide at the other side in the inversed direction. In this way, such a bi-directional  $17 \times 17$  AWG has two input waveguides and 32 output waveguides, so that it essentially functions as two identical  $1 \times 16$  AWGs.

For the present design, both the mode demultiplexer and the AWGs are designed to work with the TM polarization. Here we choose the channel spacing to be  $\Delta\lambda_{\text{ch}} = 3.2$  nm (400 GHz) and the diffraction order to be  $m = 13$  in order to ensure that the free spectral range (FSR) is large enough to cover all 16 channels, i.e.,  $\text{FSR} > N\Delta\lambda_{\text{ch}}$ . The corresponding length difference between the adjacent arrayed waveguides is  $\sim 11.547$   $\mu\text{m}$ . The length of the FPRs is chosen to be  $L_{\text{FPR}} = 100$   $\mu\text{m}$ , and correspondingly the end separation between the output waveguides is about 2.42  $\mu\text{m}$ , which is large enough to minimize the evanescent crosstalk between the output waveguides. The gap between the adjacent arrayed waveguides at the end connected to the FPRs is set at 500 nm to ensure a uniform etching depth. The width of the arrayed waveguide is designed to be 500 nm in order to be singlemode, and adiabatic tapers are introduced between the arrayed waveguides and the input/output FPRs.

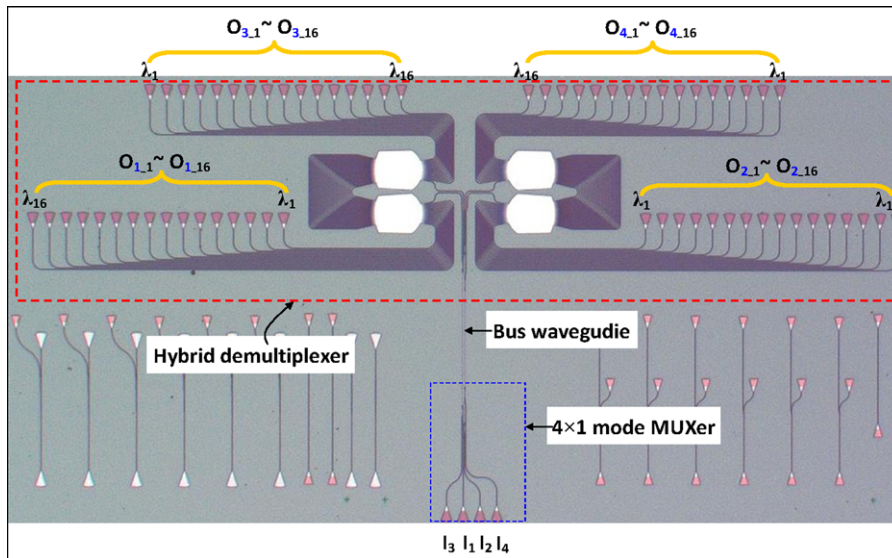


**Figure 3** The photonic integrated circuit including a  $4 \times 1$  mode multiplexer, a bus waveguide, a  $1 \times 4$  mode demultiplexer, and two bi-directional AWG demultiplexers. There are focus grating couplers connected at the input/output ends for efficient fiber-chip coupling.

The maximum width and the length for these tapers are  $1.0 \mu\text{m}$  and  $10 \mu\text{m}$  respectively.

The mode demultiplexer used here is realized with the ADC-based configuration regarding that this kind of mode demultiplexer works in a broad wavelength band and thus is WDM-compatible. The ADCs consist of a narrow access waveguide and a wide bus waveguide in the coupling region, and the key for this design is to obtain the mode-selective coupling for the  $\text{TM}_1$ ,  $\text{TM}_2$ , and  $\text{TM}_3$  modes in the wide bus waveguide, respectively, by optimizing the width of the wide bus waveguide according to the phased matching condition. The details for the ADC-type mode (de)multiplexer can be found in our previous paper [13]–[14]. For example, when the width of the narrow waveguide is set at  $w_a = 400 \text{ nm}$ , the widths of the wide waveguides in the ADCs for the  $\text{TM}_1$ ,  $\text{TM}_2$ , and  $\text{TM}_3$  modes are  $w_1 = 1.035 \mu\text{m}$ ,  $w_2 = 1.695 \mu\text{m}$ , and  $w_3 = 2.363 \mu\text{m}$ , respectively. Since the number of AWGs is reduced by half, the total size of the present hybrid demultiplexer is much smaller than the previous one with *four* AWGs reported in [22].

For the fabrication process, the chip was fabricated on a silicon-on-insulator (SOI) wafer with a  $220 \text{ nm}$ -thick top-silicon layer on a  $2 \mu\text{m}$ -thick silicon oxide layer. First an E-beam lithography process was used to make the patterned photoresist for the structure. Then an inductively coupled plasmon (ICP) etch process was conducted to fully etch the top silicon layer down to the silicon oxide layer with the patterned photoresist as the mask. Finally a PMMA thin film was formed via spin coating to protect the fabricated device. In order to characterize the present hybrid (de)multiplexer, a  $4 \times 1$  mode multiplexer is introduced at the input end of the wide bus waveguide. In this way, the desired mode-channel can be excited by launching light at the corresponding input port of the mode multiplexer. Figure 3 shows the optical microscopy image for the whole photonic integrated circuit, including the  $4 \times 1$  mode multiplexer and the present hybrid (de)multiplexer.

For the characterization process, full-etched grating couplers were used for the fiber-chip coupling, and the fibers were tiled with a tilted angle of  $10^\circ$ . A tunable laser was used as a light source, and a power-meter was used as the detector. The polarization of the input light was adjusted by a polarization controller. For measurement purposes, light was input from port  $I_1$ ,  $I_2$ ,  $I_3$ , and  $I_4$ , one by one, and correspondingly the  $\text{TM}_2$ ,  $\text{TM}_0$ ,  $\text{TM}_1$ , and  $\text{TM}_3$  modes in the bus waveguide were excited selectively by the  $4 \times 1$  mode multiplexer. After propagating through the  $200 \mu\text{m}$ -long bus waveguide, the light was then mode-demultiplexed to the  $\text{TM}_0$  modes in the narrow excess waveguides by the  $1 \times 4$  mode demultiplexer, and then the wavelength channels were separated by the cascaded AWG demultiplexers.

Figure 4(a)–(d) shows the measured responses from all 64 channels, when light is input from ports  $I_1$ ,  $I_2$ ,  $I_3$ , and  $I_4$ , respectively. These responses are normalized with the transmission response of a straight waveguide on the same chip. It can be seen that light is output dominantly from the AWG connected to output-port  $O_i$  of the mode demultiplexer when light is input from port  $I_i$  ( $i = 1, 2, 3, 4$ ), as expected. The total excess losses of the central wavelength-channels ( $O_{1,8}$ ,  $O_{2,8}$ ,  $O_{3,8}$ , and  $O_{4,8}$ ) for the four mode-channel groups are about  $3.5 \text{ dB}$ ,  $5.0 \text{ dB}$ ,  $5.5 \text{ dB}$ , and  $5.0 \text{ dB}$  when light is input from ports  $I_1$ ,  $I_2$ ,  $I_3$ , and  $I_4$ , respectively. The excess loss mainly results from two parts, i.e., the mode multiplexer and the hybrid demultiplexer (including the mode demultiplexer and the cascaded AWG demultiplexer). When light propagates from port  $I_1$  of the mode multiplexer to port  $O_1$  of the mode demultiplexer, there are only several low-loss adiabatic tapers (without any cross-coupling due to phase mismatch). Therefore, the excess loss for the transmission from port  $I_1$  of the mode multiplexer to port  $O_1$  of the mode demultiplexer is negligibly low, and the excess loss of the AWG becomes the dominant contribution. From the measured total excess losses, it can be estimated that the central channel for the AWG is about  $3.5 \text{ dB}$ . Accordingly, the excess loss for the transmission from port

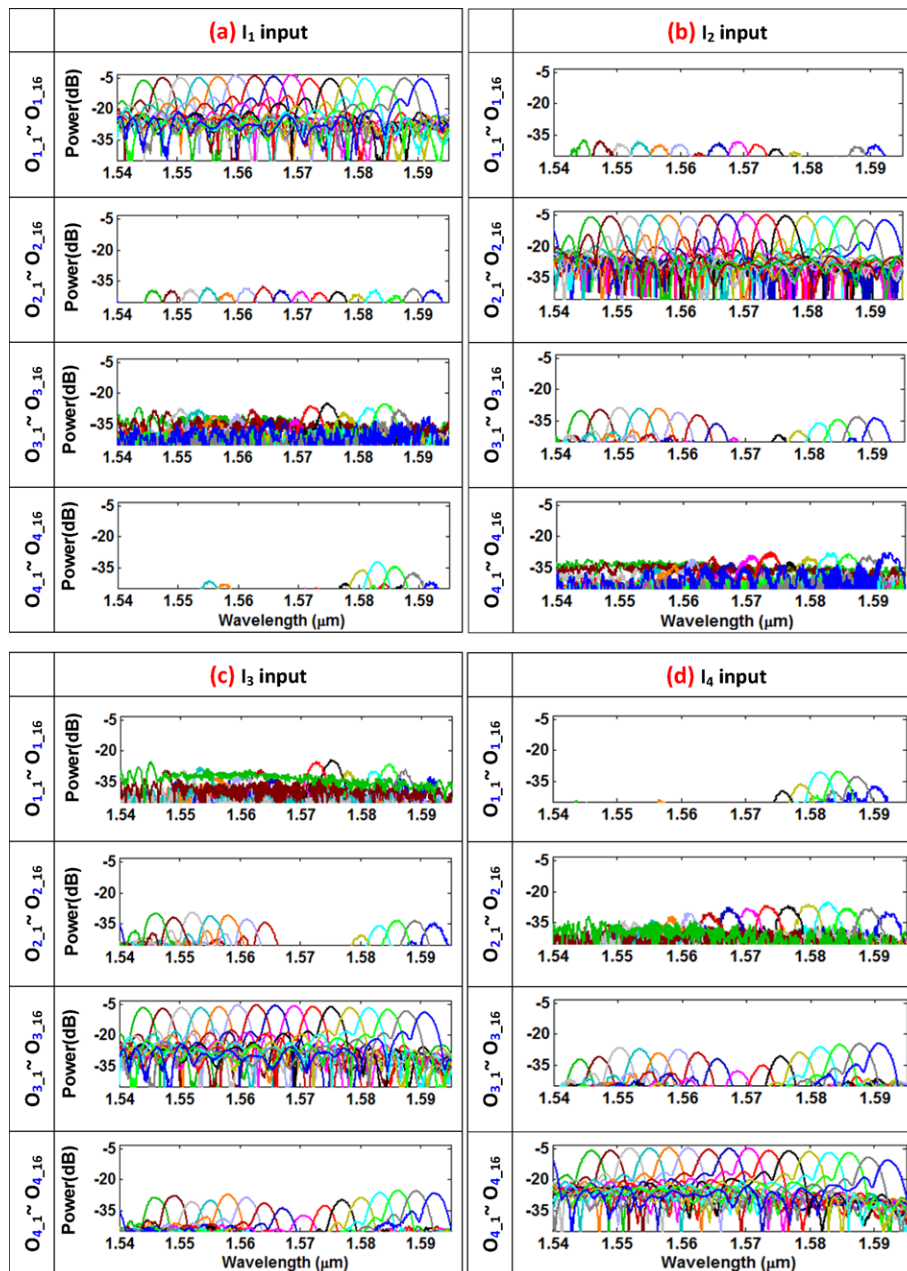


**Figure 4** Measured responses for the hybrid demultiplexer when light is input from port  $I_1$ ,  $I_2$ ,  $I_3$ , and  $I_4$ , respectively. The responses are normalized with the transmission of a straight waveguide with focus grating couplers at both ends on the same chip.

$I_i$  of the mode multiplexer to port  $O_i$  of the mode demultiplexer ( $i = 2, 3, 4$ ) is about  $\sim 1.5$  dB. Figure 4(a)–(d) also show that the transmissions for channels  $O_{i-1} \sim O_{i-16}$  ( $i = 1, 2, 3, 4$ ) are quite uniform and the non-uniformity is less than 2 dB, which is similar to the channel non-uniformity of a single AWG fabricated on the same chip. This indicates that the present ADC-type mode (de)multiplexer has a broad band to cover all the AWG channels (ranging from 1540 nm to 1590 nm) and thus is WDM-compatible, as verified in our previous paper [14].

From Fig. 4(a)–(d), it can also be seen that the present hybrid demultiplexer has crosstalks of  $< -20$  dB between the mode channels, which is also similar to the performance of a single mode (de)multiplexer demonstrated in Ref. [14].

The crosstalk between the wavelength channels is relatively large ( $\sim -14$  dB), which is due to the phase errors in the bi-directional AWG (de)multiplexer. It can be seen that the performances of the bi-directional AWG presented here is similar to the regular AWG shown in our previous paper [22]. The present hybrid demultiplexer should work well according to the realization of error-free transmission (bit error rate  $< 10^{-12}$ ) using a microring multiplexer with a crosstalk of  $\sim -13$  dB demonstrated in Ref. [19]. It is possible to further improve the performances (e.g.,  $< -20$  dB crosstalk) for the bi-directional AWG by introducing wide arrayed waveguides to minimize the phase errors from fabrication imperfections [26], and thus realize an excellent hybrid demultiplexer in the future.

### 3. Conclusion

In summary, we have proposed a novel silicon hybrid demultiplexer to realize WDM and MDM simultaneously by introducing  $(N + 1) \times (N + 1)$  bi-directional AWGs so that the number of the AWGs is reduced by half and the footprint for the hybrid demultiplexer is also reduced greatly. As an example, a compact 64-channel MDM-WDM hybrid demultiplexer based on SOI nanowires has been realized by utilizing a  $1 \times 4$  ADC-type mode demultiplexer with four mode-channels and two  $17 \times 17$  bi-directional AWGs with 16 wavelength-channels. Each  $17 \times 17$  bi-directional AWG is equivalent to two identical  $1 \times 16$  AWGs. For the fabricated device, the excess loss is  $3.5 \sim 5$  dB while the wavelength-channel crosstalk and the mode-channel crosstalk are about  $-14$  dB and  $< -20$  dB, respectively. Better performance can be achieved by minimizing the imperfections (particularly in AWGs) during the fabrication processes in the future.

**Acknowledgements.** This project was partially supported by a 863 project (No. 2011AA010301), the Nature Science Foundation of China (No. 6141101056, 11374263, and 61422510), the Doctoral Fund of Ministry of Education of China (No. 20120101110094).

**Received:** 4 December 2014, **Revised:** 20 March 2015,

**Accepted:** 9 April 2015

**Published online:** 30 April 2015

**Key words:** mode, wavelength, multiplexing, arrayed-waveguide grating (AWG) asymmetric directional coupler.

### References

- [1] D. Dai and J. E. Bowers, *Nanophoton.* **3**, 283–311 (2014).
- [2] A. Alduino, L. Liao, M. R. Jones, et al. in *Integrated Photonics Research, Silicon and Nanophotonics and Photonics in Switching*, OSA Technical Digest (CD) (Optical Society of America, 2010), paper PDIW15.
- [3] D. J. Richardson, J. M. Fini, and L. E. Nelson, *Nature Photon.* **7**, 354–362 (2013).
- [4] R. G. H. van Uden, R. Amezcua Correa, E. Antonio Lopez, F. M. Huijskens, C. Xia, G. Li, A. Schülzgen, H. de Waardt, A. M. J. Koonen, and C. M. Okonkwo, *Nature Photon.* **8**, 865–870 (2014).
- [5] Y. Kawaguchi and K. Tsutsumi, *Electron. Lett.* **38**, 1701–1702 (2002).
- [6] T. Uematsu, Y. Ishizaka, Y. Kawaguchi, K. Saitoh, and M. Koshiba, *J. Lightwave Technol.* **3**, 2421–2426 (2012).
- [7] J. Xing, Z. Li, X. Xiao, J. Yu, and Y. Yu, *Opt. Lett.* **38**, 3468–3470 (2013).
- [8] N. Riesen and John D. Love, *Appl. Opt.* **51**, 2778–2783 (2012).
- [9] J. D. Love, R. W. C. Vance, A. Joblin, *Opt. Quant. Electron.* **28**, 353–369 (1996).
- [10] W. Chen, P. Wang, and J. Yang, *Opt. Express* **21**, 25113–25119 (2013).
- [11] M. Greenberg and M. Orenstein, *Opt. Express* **13**, 9381–9387 (2005).
- [12] S. Bagheri and W. M. J. Green, in *Proceedings of IEEE Group IV Photonics Conference (San Francisco, United States of America, 2009)*, 166–168.
- [13] D. Dai, in *Asia Communications and Photonics Conference, (Guangzhou, China, 2012)*, ATH3B.3.
- [14] D. Dai, J. Wang, and Y. Shi, *Opt. Lett.* **38**, 1422–1424 (2013).
- [15] Y. Ding, J. Xu, F. Da Ros, B. Huang, H. Ou, and C. Peucheret, *Opt. Express* **21**, 10376–10382 (2013).
- [16] H. Qiu, H. Yu, T. Hu, G. Jiang, H. Shao, P. Yu, J. Yang, and X. Jiang, *Opt. Express* **21**, 17904–17911 (2013).
- [17] J. Wang, S. He, and D. Dai, *Laser Photon. Rev.* **8**, L1–L5 (2014).
- [18] J. Wang, P. Chen, S. Chen, Y. Shi, and D. Dai, *Opt. Express* **22**, 12799–12807 (2014).
- [19] L.-W. Luo, N. Ophir, C. P. Chen, L. H. Gabrielli, C. B. Poitras, K. Bergmen, M. Lipson, *Nat. Commun.* **5**, 3069 (2014).
- [20] J. Driscoll, C. Chen, R. Grote, B. Souhan, J. Dadap, A. Stein, M. Lu, K. Bergman, and R. Osgood, *Opt. Express* **22**, 18543–18555 (2014).
- [21] Y. Yang, Y. Li, Y. Huang, and A. Poon, *Opt. Express* **22**, 22172–22183 (2014).
- [22] J. Wang, S. Chen, and D. Dai, *Opt. Lett.* **39**, 6993–6996 (2014).
- [23] Y. Tachikawa, Y. Inoue, M. Ishii, and T. Nozawa, *J. Lightwave Technol.* **14**, 977–984 (1996).
- [24] M. K. Smit, and C. V. Dam. *IEEE J. Sel. Top. Quant. Electron.* **2**, 236–250 (1996).
- [25] W. Bogaerts, D. Taillaert, P. Dumon, D. V. Thourhout, and R. Baets, *Opt. Express* **15**, 1567–1578 (2007).
- [26] S. Pathak, D. Van Thourhout, and W. Bogaerts, *Opt. Lett.* **38**, 2961–2964 (2013).